JPCCCK

APRIL 4, 2013
VOLUME 117
NUMBER 13

pubs.acs.org/JPCC

THE JOURNAL OF PHYSICAL CHEMISTRY C

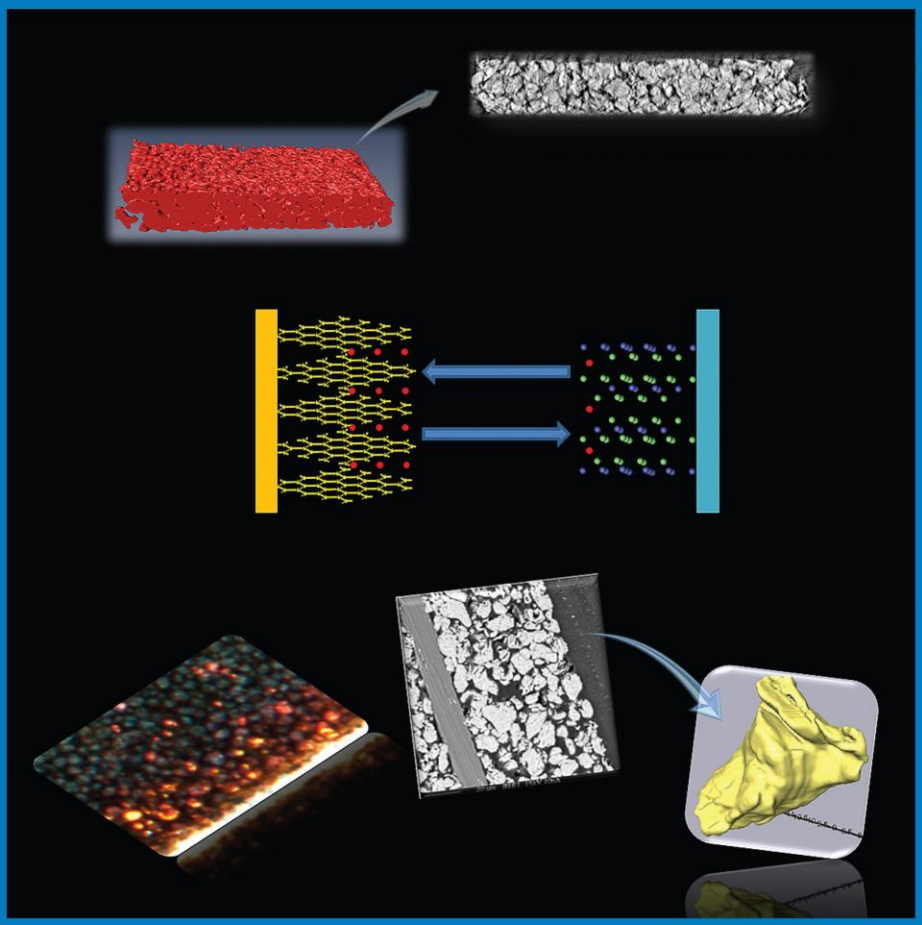

Mesoscale Complexity and Inhomogeneity in Li-ion Batteries (see page 5A)

ENERGY CONVERSION AND STORAGE, OPTICAL AND ELECTRONIC DEVICES, INTERFACES, NANOMATERIALS, AND HARD MATTER

ACS Publications
MOST TRUSTED. MOST CITED. MOST READ.

www.acs.org

THE JOURNAL OF PHYSICAL CHEMISTRY C

Feature Article

pubs.acs.org/JPCC

Effects of Inhomogeneities—Nanoscale to Mesoscale—on the Durability of Li-Ion Batteries

Stephen J. Harris[†] and Peng Lu*[,‡]

[†]Materials Science Division, Lawrence Berkeley National Lab, Berkeley, California 94720, United States

[‡]Chemical & Materials Systems Lab, General Motors R&D Center, Warren, Michigan 48090, United States

ABSTRACT: We review work from our laboratory that suggests to us that most Li-ion battery failure can be ascribed to the presence of nano- and microscale inhomogeneities that interact at the mesoscale, as is the case with almost every material, and that these inhomogeneities act by hindering Li transport. (Li does not get to the right place at the right time.) For this purpose, we define inhomogeneities as regions with sharply varying properties—which includes interfaces—whether present by "accident" or design. We have used digital image correlation, X-ray tomography, FIB-SEM serial sectioning, and isotope tracer techniques with TOF-SIMS to observe and quantify these inhomogeneities. We propose new research approaches to make more durable, high energy density lithium-ion batteries.

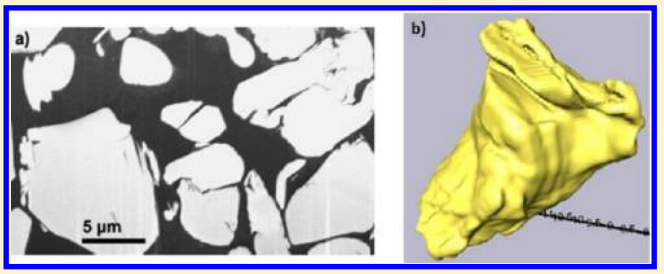

INTRODUCTION

Since their invention,[1−3] Li-ion batteries have become ubiquitous in consumer electronics. Over the two decades since their introduction,[4] battery chemistry has changed little, with most consumer batteries still using the original $LiCoO_2$ positive electrodes ("cathodes") and graphite negative electrodes ("anodes"). Yet, through innovative packaging and engineering design, their energy densities have more than doubled. The ability to improve battery design has been due largely to the porous electrode, macrohomogeneous model developed and refined by Newman and others[5−21] over two decades. The model allowed battery designers to make trade-offs[22] between, for example, electrode thickness, porosity, power, and energy density. By the mid 2000s, billions of Li-ion batteries were being manufactured each year, and it may well have seemed that Li-ion battery technology had matured. For example, battery life of 2 or 3 years was well-matched to the requirements of cell phones and laptops; the batteries had acceptable abuse tolerance; energy density was adequate; and the cost was accepted by consumers.

Some of the assumptions made by the macrohomogeneous model include:

- Electrodes are homogeneous, so they have single, time-independent effective values for particle size, porosity, tortuosity, and transport coefficients.
- Li^+ transport within the porous electrode is 1-dimesional.
- Li^+ transport within individual particles is 1-dimensional (radial). Particles are spherical. The local state of charge (SOC) in a particle is constant on any radius (shrinking core model).
- Particles have no internal structure, porosity, or defects. Therefore, the electrolyte cannot penetrate into the particles, and Li transport within them is solely by bulk diffusion.
- Particles are small compared to the electrode thickness and to the scale of $[Li^+]$ gradients, so that the $[Li^+]$ in the electrolyte is constant on the surface of each particle.
- The properties of the binder[23−26] and the conductive carbon,[27] while of considerable importance, can be absorbed into other transport or chemical parameters in the model.

It was, of course, recognized that these assumptions are far from perfect, and modeling extensions of Newman's approach appeared, including studies of effects of inhomogeneities.[16,21,28−35] But there was only a very modest experimental effort aimed at analyzing the effects of inhomogeneities,[36−47] and the original homogeneous model is still widely used. Perhaps this is because inclusion of microstructural details and local variability makes the codes much more expensive to run, while the original, homogeneous model was very successful in describing battery performance.

In the late 2000s, governments substantially increased funding aimed at the ultimate goal of an electrified vehicle fleet.[48] This goal requires addressing some of the following concerns:

- Safety is paramount, requiring stricter limitations on the choice of electrode materials. (It is curious that the combustion community has not played a role here.[49])
- Battery life has to be extended to 10−15 years to meet cost and regulatory requirements.

Received: November 19, 2012
Revised: January 28, 2013
Published: February 8, 2013

   dx.doi.org/10.1021/jp311431z | J. Phys. Chem. C 2013, 117, 6481−6492

- Batteries must start a vehicle at −30 °C, and they must accept regenerative braking energy at high rates. Recharging time must be dramatically reduced.
- Energy per dollar has to increase by more than a factor of 2 in order for plug-in hybrid and all-electric vehicles to be commercially viable.
- Volumetric energy density must increase dramatically to provide a range—perhaps 200 miles—that will satisfy customers of all-electric vehicles.
- Recycling, never significant for cell phone, camera, or laptop batteries, will have to be implemented.[50−52] Life cycle analyses will be necessary to make optimal trade-offs between upfront costs and recycling value of expensive materials such as Co.
- Replacement of limited-resource materials such as copper may be necessary.
- The possibility of battery rejuvenation will have to be considered.

Among these challenges, battery durability is especially tightly coupled to the others because today's automotive batteries are significantly oversized to achieve the required life. Thus, a more durable battery technology would automatically enable batteries with smaller size and weight for the same energy (higher energy density). In turn, smaller, lighter batteries would require less upfront and recycling costs and provide improved range and safety. We argue below that inhomogeneities in batteries—just like inhomogeneities in practically all materials—are the primary drivers of failure, so that in at least some cases, a purely homogeneous model will not be able to predict durability. Instead, we suggest that a detailed understanding of the electrode structures and *in*homogeneities at all scales, from nano- to mesoscale (where inhomogeneities interact), can lead to an improved understanding of durability and failure mechanisms, ultimately leading to longer-lived batteries, with all their attendant advantages.

In this paper we review research from our laboratory. Our goal is to provide a better understanding of the fundamental processes that lead to degradation and failure in Li-ion batteries. This understanding has suggested a new approach to us for improving battery durability. We will conclude by suggesting that this same new approach for longer life batteries can also be used to increase their energy density without decreasing power density.

BACKGROUND

Following Huggins,[53] we consider two materials AB and C that can react according to

$$AB + C \rightarrow A + BC \tag{1}$$

with free energy change ΔG. The sign of the free energy change indicates the direction of the spontaneous reaction, and the magnitude of the free energy change indicates the thermodynamic driving force for the reaction. We submerge AB and C (the electrodes) in an electrolyte (a filter that blocks electron transport while allowing ions to pass) and connect them to each other with an external conducting wire (a filter that blocks ion transport while allowing electrons to pass). Under these conditions, Reaction 1 might take place via

$$AB + C \rightarrow A + B^+ + e^- + C \rightarrow A + BC \tag{2}$$

where B^+ travels to C through the electrolyte and the electron travels to C through the wire. A voltmeter placed across the electrodes when the circuit is open will measure a voltage difference ("open circuit voltage", OCV) that also indicates the direction of the spontaneous reaction and the magnitude of the thermodynamic driving force. Thus, voltage and free energy change must be closely related, and this relationship is given by[3]

$$\Delta G = -nFE \tag{3}$$

where E is the measured voltage; n is the number of electrons transferred; and F is Faraday's constant. If we replace B with "Li", A with "negative electrode", and C with "positive electrode", and if we prevent the electrodes from touching each other with a separator (typically a 20 μm thick layer of porous polypropylene), we have a Li-ion battery. In cases where Li makes a strong bond (>4 V for $LiCoO_2$), then its free energy is low, and its voltage is high (from eq 3)—so $LiCoO_2$ is a positive electrode material. In cases where Li makes a weak bond (~0.1 V for a Li^+ intercalated in graphite), then its free energy is high, and its voltage is low—so graphite is a negative electrode material. This cell, like many Li-ion cells, has an OCV near 4 V, higher in general than cells made from any other material.

When we charge this cell, we force electrons (e.g., with a power supply) from the positive to the negative electrode. Li^+ ions are repelled by the positively charged electrode and dissolve into the electrolyte solution, where they can travel toward and insert into the negative electrode. Thus, in the battery's charged state, Li-ions have been removed from their low energy state and pushed into a high energy state, storing energy. Replacing the power supply with a light bulb allows the Li (and associated electrons) to return to the positive electrode, and the stored energy is extracted. To the extent that there are no parasitic reactions that consume Li, the ratio of the number of electrons (or Li ions) retrieved during discharge to the number of electrons used during charge (the "Coulombic efficiency") is 1.[54] In fact, a Coulombic efficiency of about 0.99995 is required in order for an automotive battery to survive (retain 80% of initial capacity) for the required 5000 cycles (once a day for 15 years), while a Coulombic efficiency of 0.999—not often achieved with cells made in academic research laboratories—is unacceptable for most commercial uses because it would have a 20% capacity loss after just 200 cycles. (As Dahn has pointed out,[55] the fact that commercial cells may be 1−2 orders of magnitude more durable than laboratory cells is worth thinking about when analyzing published durability studies.) On the other hand, the amount of energy extracted during discharge is necessarily lower than the amount of energy stored, depending on the current and the battery's internal resistance.

Another important process has to do with the fact that the electrolyte solutions (typically 1 M $LiPF_6$ dissolved in an ethylene carbonate−diethyl carbonate mixture) are not thermodynamically stable at either high (>4 V) or low voltages (<1 V). The result is that degradation films deposit on the electrodes. These deposits, formed from oxidation or reduction products at the electrodes, are made of insoluble Li salts. On the negative electrode, the deposits form a Li^+-conductive but electronically insulating thin film called the Solid Electrolyte Interphase (SEI).[10,12,55−83] The SEI formation process irreversibly consumes Li until it is sufficiently thick (perhaps 10−20 nm) so that the electrode no longer reduces the electrolyte. Deposits on the positive side may not conduct Li^+, and this would lead to cell failure. Thus, while 5 V positive electrode materials exist,[84] we cannot take advantage of them until more oxidation-resistant electrolytes or better protective coatings are found.[85]

SEI films protect the electrolyte from further reduction and concomitant loss of capacity (Li loss) while allowing Li^+ to

dx.doi.org/10.1021/jp311431z | J. Phys. Chem. C 2013, 117, 6481−6492

transport through them. Battery degradation is often due to failure of the SEI to perform one or both of these two required functions, leading to loss of capacity and/or an increase of internal impedance. In a full cell (i.e., not using a Li metal negative electrode), such as $LiCoO_2$ vs graphite, up to 10% of all the Li in the cell is irreversibly consumed in forming the SEI, which translates to a 10% reduction in cell capacity during the first cycle. SEI formation is a particularly significant problem for nanomaterials because the amount of SEI formed (loss of Li) scales with the electrode surface area.[55] Since nanomaterials have very high surface areas, they must in general be avoided as negative electrode materials. (They can always be studied in half cells, where there is an unlimited supply of Li, but half cells have no commercial value.) Nanomaterials face other challenges in practical battery anodes, including the fact that they are often difficult to pack with acceptable volumetric density.

Once the lithiated graphite reaches the empirical formula LiC_6, it is "full", in that no additional Li will insert. Additional electrons pumped to the graphite react with Li^+ to form electroplated Li metal, which must be avoided because it does not form a stable (protective) SEI and because it grows dendrites that can puncture the separator and cause a short circuit.[86]

BATTERY DEGRADATION AND FAILURE: A HIGH LEVEL VIEW

A barrier to understanding degradation and failure in Li-ion batteries has been the large number of failure modes that are possible, including processes involving chemical, mechanical, electrical, and morphological changes. For example, Kostecki and McLarnon[87] showed that conductive carbon in an electrode can coagulate or change chemically with age, leaving some areas of the electrode electrically disconnected. Theirs may have been among the first published demonstrations[88,89] that microscale inhomogeneities, not accounted for in the macrohomogeneous models, can play a controlling role in battery degradation. However, we note that loss of internal electrical connectivity has also been attributed to particle fracture,[90−92] to precipitation of thick surface films,[93−95] to gas generation,[96] to loss of contact between active material and the current collector,[97] to loss of contact between the current collector and the cell housing,[19] and to degradation of the binder.[98] Demonstrating whether any of these processes actually causes macroscale degradation for a particular cell requires the sort of microscale-to-mesoscale measurements that are not often made.

To find a high level organizing principle to approach the subject of battery durability, we looked for processes common to most failure modes and offered two hypotheses:[99−101]

1. In an ideal Li-ion battery, the only steps that should occur are Li moving back and forth between and into the electrodes. Thus, fundamental studies of battery degradation could begin by asking where the Li is and where it is going, based on the hypothesis[99] that in a failed battery the Li is not going to the right place at the right time.

2. Materials do not in general fail homogeneously; instead, nano- and microscale inhomogeneities interact at the mesoscale to cause failure.[102−108] We hypothesize[101] that battery failure is the result of interactions among local inhomogeneities—mechanical, electrical, morphological, or chemical. (For the purposes of our work, we define inhomogeneities as regions with sharply varying properties—which includes interfaces—whether present by "accident" or design.)

If we accept these hypotheses, then experimental degradation research could focus on comparing in situ, time-dependent, spatially resolved Li maps—in the electrolyte and in the active material—in fresh and degraded systems that have *well-characterized microstructures and inhomogeneities*. Simultaneously, modeling research on degradation could focus on understanding and interpreting the impact of local inhomogeneities on transport and reactivity in such systems. In our work, described in the next section, we have tried to follow this line of thinking. However, we note that until recently, there were no in situ Li maps, no in situ strain maps, no 3D electrode or particle data, no models dealing with real 3D data, no determinations of how Li transports through the SEI, and in general only a very modest interest in how nano- and microscale inhomogeneities might interact to cause failure at the mesoscale.

LI TRANSPORT AND INHOMOGENEITIES

Optical Methods. Spatially resolved in situ maps of Li in an electrode can provide useful information about Li transport, and optical techniques are among the simplest. We take advantage of the fact that graphite changes color as it lithiates. When the empirical formula of lithiated graphite reaches LiC_{18}, it turns dark blue from gray/black; when the formula reaches LiC_{12}, it turns red; and when the formula reaches the fully lithiated LiC_6, it turns gold.[44,109] With this technique, Maire et al.[44] showed a graphite electrode that failed heterogeneously, with variations in SOC on a scale of millimeters. Such heterogeneous failure suggests different remediation strategies than would homogeneous failure.

A more quantitative version of this color strategy was used by Novak's group and by us[110,111] to make the first in situ time-dependent (local SOC-dependent) maps of Li in battery electrodes. A sequence of images, viewed from above, of a graphite electrode in a half cell from our lab is shown in Figure 1, while the corresponding video can be seen online.[112] The images show the "southern" edge of the graphite electrode through the sapphire window of an optical cell; the counter Li metal electrode

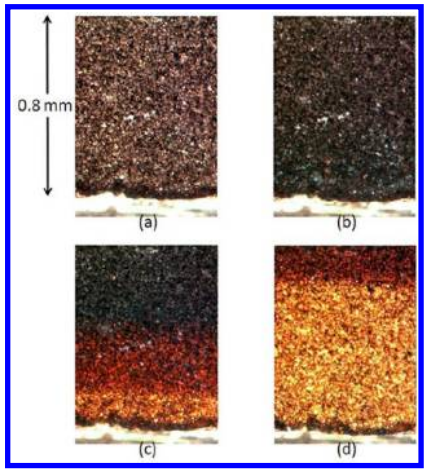

Figure 1. Sequence of four optical micrographs showing the time evolution of color in a graphite electrode, with Li traveling from the "southern" edge traveling "north", lithiating as it goes. (a) Initial, delithiated. (b) Graphite mainly in the blue, dilute stage 2; taken after approximately 6 h of lithiation. (c) Three graphite stages visible: blue (dilute stage 2), red (stage 2), and gold (stage 1); taken approximately 3 h after the image shown in (b). (d) Two graphite stages visible: red (stage 2) and gold (stage 1); taken approximately 4 h after the image shown in (c). Videos showing the time dependence of the lithiation process are available on the Internet at www.LithiumBatteryResearch.com.

dx.doi.org/10.1021/jp311431z | J. Phys. Chem. C 2013, 117, 6481−6492

was off screen to the south. Li^+ ions transported from the Li metal into the graphite, south to north, bringing the graphite into successively more lithiated states—from blue to red to gold. (Colors have been enhanced with Photoshop to make them more obvious.)

Images like this can provide a variety of new insights about Li^+ transport, beyond simply measuring the transport rate in a particular electrode. In one example,[113] we used the fact that active particles in graphite electrodes swell by about 10% in volume as they lithiate in order to answer the following question: How is the extra swelling volume accommodated in the electrode? At one extreme, the porosity of the electrode could remain constant so that the electrode volume increases upon lithiation. At the other extreme, the electrode volume could remain constant so that the porosity decreases upon lithiation.[15,114] We used digital image correlation (DIC) techniques to show that the average strain of the electrode was only about 0.2% during lithiation, an order of magnitude smaller than the strains of individual graphite crystallites.[115] This result implies that most of the swelling goes into reducing porosity. For an electrode with porosity of 40%, perhaps a quarter of that is lost during charging, contradicting the usual implicit assumption that porosity and, therefore, tortuosity, conductivity, and diffusivity, are constant during cycling. A spatially inhomogeneous loss in porosity could have a strong impact on local porosity, perhaps closing off important transport pathways. DIC also showed us that the more lithiated (gold) areas of the electrode compressed the less lithiated (blue) areas, even though both phases "want" to expand as they lithiate, confirming Qi's earlier prediction[116] that the modulus of lithiated graphite increases with lithiation.

Li maps also allowed us to test the shrinking core model.[117−119] Although obviously inapplicable to anisotropic single-crystal particles such as $LiFePO_4$, the assumption of internal particle isotropy, fundamental to the shrinking core model, has been almost universally adopted in models of polycrystalline particles—in effect, assuming that internal structures are randomly oriented and sufficiently small compared to the particle size so that particle interiors could be treated as isotropic on the particle scale. However, the fact that effective bulk diffusion coefficients extracted by different researchers using shrinking core model analyses vary by some orders of magnitude for graphite[120] already suggests that this assumption may be a poor one. Images of the interior of ~10 μm diameter graphite and $LiCoO_2$[100] particles in Figure 2 suggest why: the internal grains for these layered materials are in fact not especially small compared to the particle size, so that internal variability does not necessarily average out. Furthermore, the presence of internal porosity suggests that calculations of internal stress and fracture strength made without some knowledge of its interior microstructure may be of limited validity.[100] A particle's performance thus depends not only on fundamental properties of graphite but also on the way its nano- and micro-scale internal subunits are oriented and connected to each other at the mesoscale.

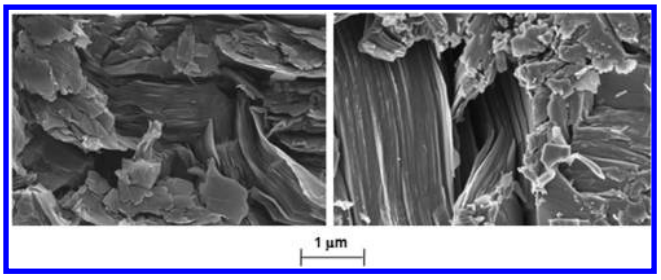

Figure 2. SEM images of cross sections of a focused ion beam (FIB)-cut graphite particle (left) and a FIB-cut $LiCoO_2$ particle (right) taken from the same commercial battery. The internal structures, with characteristic structure and pore sizes of −2 μm and above, are not especially small compared to the dimensions of the particles, about 10 μm.

The isotropy assumption predicts that the state of charge on the surface of a spherical particle must be uniform. That translates to a prediction for spherical graphite particles that their external surfaces are monochromatic (gray/black, blue, red, or gold). Our in situ optical images[119,121] of lithiating ~10 μm spherical mesocarbon microbeads (MCMBs) show instead that particles lithiate gradually from "hot spots" that expand over the surface until they cover the particle (Figure 3). This observation is readily rationalized using a microstructural model of MCMB particles in which the hot spot location depends on the internal microstructure of the graphite.[119]

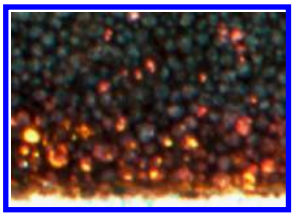

Figure 3. SOC variation on the surface of individual spherical particles; some regions in particle form hot spots (intensely colored areas). These hot spots expand until particles are fully lithiated. Note also that while the average state of charge is highest near the "southern" edge there is widespread variability in the local state of charge.

Three-Dimensional Techniques. A more detailed understanding of transport among and within particles requires 3D structural data.[101,122−126] Two of the most powerful approaches for obtaining 3D information are tomography and serial sectioning. Each technique has advantages and limitations, and with either technique, a trade-off must be made between higher spatial resolution and larger field of view. The former may be appropriate for studying the internal structures of a small number of particles, while the latter may be required for analyzing statistically significant volumes—that is, volumes large enough to be representative for a particular property such as porosity.[124]

X-ray Tomography. In our initial X-ray tomography (or nano-CT) work[122] we examined the graphite electrode from a commercial laptop battery. We reconstructed an 86 μm (electrode thickness) × 348 μm × 478 μm sample with voxel (3D pixel) dimensions of 480 nm (Figure 4a) and focused on identifying homogenization scales. We define the homogenization scale for a particular parameter, such as the volume-specific surface area, as the smallest representative volume element (RVE) for which the parameter value does not depend strongly on the volume element size or location. The standard deviation of the volume-specific surface area was about ±50% for volume elements with dimensions 11 μm × 15 μm × 15 μm, containing just a few particles. For volume elements at least 45 μm × 60 μm × 30 μm, containing perhaps 50−100 particles, the standard deviation was less than ±15%. This result suggests that an RVE in a finite element (FE) calculation built from 10 μm particles should have ~100 particles for the internal surface area to be represented accurately. Naturally, the minimum RVE size depends strongly on the parameter that is being represented.

dx.doi.org/10.1021/jp311431z | J. Phys. Chem. C 2013, 117, 6481−6492

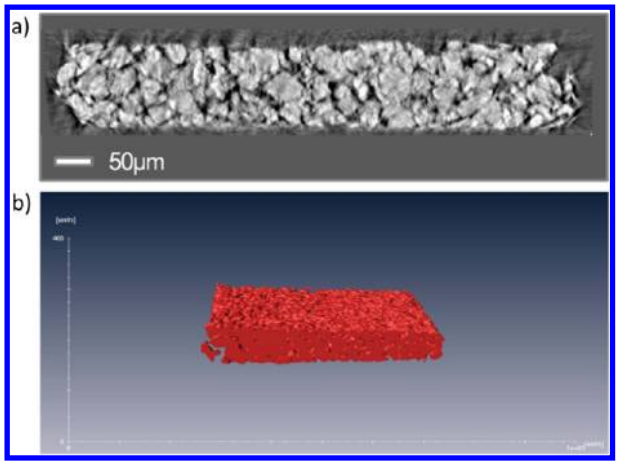

Figure 4. (a) Individual slice from the X-ray tomography sequence of a commercial graphite electrode. (b) Rendering of 300 individual tomography slices (dimensions 43 × 348 × 144 μm).

For tortuosity, even our entire sample appears not to be large enough.

Tortuosity[127] τ is not uniquely defined in three dimensions, but in the battery field it is taken to be the parameter that connects porosity ε to transport parameters. It is defined by the equation

$$D^{\text{eff}} = \left(\frac{\varepsilon}{\tau}\right) D^{\text{bulk}}$$

where D^{bulk} is the Li^+ diffusion coefficient in bulk electrolyte and D^{eff} is the effective diffusion coefficient for transport through the pores of an electrode. The same value of τ is used to scale the conductivity. τ can be fit to transport data, typically taking a value in the range 3[128] to 5,[129] or it can be estimated based on an assumed relationship with porosity. In the battery field the (modified) Bruggeman relationship

$$\tau \propto \frac{1}{\varepsilon^{0.5}} \quad \text{or} \quad \tau \propto \frac{A}{\varepsilon^{B}}$$

is used, but Shen and Chen[130] list about a dozen such relationships. They all have in common the property that, for random pore arrangements, tortuosity increases when porosity decreases. Finally, if the full 3D electrode microstructure is known, τ can be evaluated with an FE or other type of analysis,[131] comparing the calculated transport time through the electrode with the calculated transport time through the same distance in the absence of the electrode.[101,132]

The possibility that local variability in tortuosity could be important has only recently been raised in the Li battery literature,[101] although it has been analyzed in other fields.[131,133] To quantify the variability, we divided the graphite electrode into subregions of about 43 μm (thick) × 80 μm × 100 μm and calculated the tortuosity for each of them. The results of our FE calculations for 12 such subregions are shown in Figure 5. Although the resolution of 480 nm is not sufficient to resolve the smaller pores, Landau[127] demonstrated that the tortuosity is determined primarily by the larger pores since they carry nearly all of the current from the front to the back of the electrode. (The nanopores can, however, have a large influence on the local kinetics.)

We suggest that there is a significant impact on battery durability from the outlier subregions shown in Figure 5. Subregions such as #3, which have especially high tortuosities,

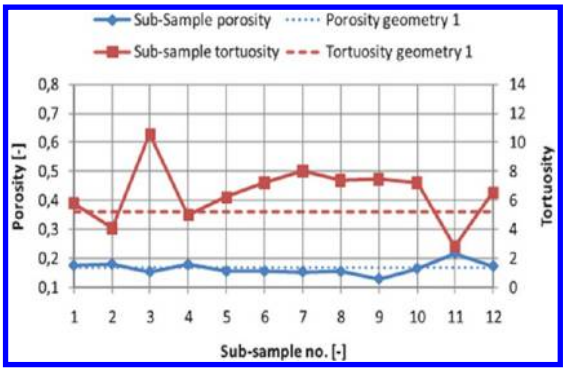

Figure 5. Calculated porosity and tortuosity for 12 subregions (43 μm × 80 μm × 100 μm) from the graphite electrode shown in Figure 4.

will be avoided by approaching Li^+ ions, leading to inefficient charging and discharging there. As a result, the rest of the electrode will experience a higher than average current density, which lowers its capacity and life. On the other hand, subregions such as #11, which have especially low tortuosities, will be sought out by approaching Li^+ ions and will experience high current densities (in the example shown about twice the average). Cells run at high current density inevitably show decreased capacity and degrade prematurely, by local plating on the negative electrode (Plating occurs at negative local overpotentials. Different from plating on a metal surface, Li plating occurs in competition with insertion, which is an activated process, so plating is more likely to occur at low temperatures.) or by local overcharging (electrolyte oxidation or damage to the active material) on the positive electrode. Thus, the specified maximum safe current density and SOC are reduced for a cell with heterogeneous electrodes to avoid failure at outlier points.

While tortuosity variability will certainly lead to variability in the local current density, the magnitude of the impact can best be evaluated with an electrochemical model of a real electrode.[134] The first electrochemical model capable of importing real 3D data was built by Garcia et al.[123] and was used to assess the importance of microstructural inhomogeneities on mesoscale transport in our graphite electrode. The analysis predicts the existence of at least three microstructural populations within the electrode, namely, (1) a dendrite-favoring population, (2) a mean field population, and (3) an electrochemically isolated population. The analysis also shows that surface roughness and features with a small radius of curvature favor lithium accumulation, low galvanostatic potentials, and dendrite nucleation and growth. The same features also favor mechanical failure from high stress. Surface grains oriented along the low diffusivity axis will significantly increase the risk for lithium deposits and localized tensile states of stress. In addition, closed pores increase the macroscopic electrical impedance of the electrode and suppress the local lithium diffusivity. At moderately high current densities, Garcia et al. calculated that up to 50% of the electrode could be isolated or could develop dangerously low electrochemical potentials, demonstrating that tortuosity variability is a critical aspect in electrodes, affecting not only the macroscopic power density but also the long-term durability.

FIB-SEM. Serial sectioning using a focused ion beam with SEM imaging (Focused Ion Beam Scanning Electron Microscope, FIB-SEM) provides resolution limited only by the SEM. With an electron backscatter diffraction (EBSD) attachment, the internal grain structures and orientations are available,[126] and with EDX

dx.doi.org/10.1021/jp311431z | J. Phys. Chem. C 2013, 117, 6481−6492

local composition can be determined[135] (although the most important species, Li, is not detectable this way). One obvious drawback is that the technique is destructive. A more subtle difficulty is that it is not in general possible to reconstruct a 3D porous material from a series of 2D images because the surface of a cut through a porous material is rough. Thus, different pixels in a single 2D image may refer to material at different heights, violating an assumption of the reconstruction algorithm. The most common solution is to fill the pores with an epoxy or other material so that the sample is no longer porous, and all pixels in an image refer to points at the same height. If the sample material is distinguishable from the epoxy in the 2D images, and if the insertion of the epoxy does not change the microstructure, then a faithful 3D reconstruction is possible.

In our work we examined a $LiCoO_2$ electrode[126] from the same battery as the graphite electrode discussed above. Because of the high spatial resolution used here, only a relatively small volume was interrogated, but we obtained a detailed view of the particle shapes and internal microstructures. Two related observations stand out. First, the presence of (black) epoxy threading its way through particles demonstrates that the electrolyte has access to particle interiors[126,135] via cracks, even in this brand new cell (Figure 6a), although transport through the bulk and through mesopores is likely also taking place. Second, we found that the particle shapes are much more complex than might be inferred from looking at 2D images. On the whole, these particles appear convex in Figure 6a, suggesting that ellipsoids could be a good approximation to their shapes. However, this impression is an illusion because it does not take into account that many of these 2D "ellipses" are actually connected in the third dimension. Thus particles can have large concave surfaces and deep crevices, such as the particle shown in Figure 6b, which is reconstructed directly from images like Figure 6a. On the basis of these two observations, together with the images in Figure 2, it is clear[120] that transferable solid phase diffusion coefficients cannot in general be extracted from a simple 1D analysis of the kinetics of lithiation.

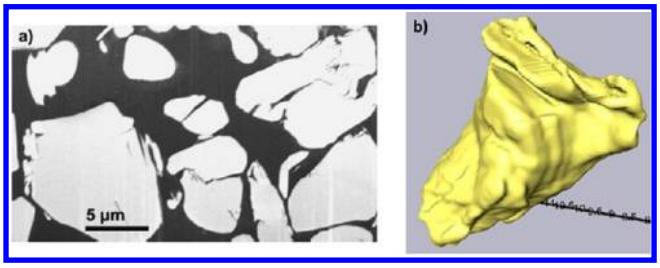

Figure 6. (a) SEM image of a cross section of a $LiCoO_2$ electrode. Black areas show the location of the epoxy added to the electrode for purposes of making the FIB-SEM images. Note that the epoxy can enter the interior of the particles. (b) Three-dimensional reconstruction from (a) of an individual $LiCoO_2$ particle. Note the presence of deep crevices and other concave regions that are not obvious from the 2D cross section.

Isotope Tracer Experiments. As previously mentioned, SEI films have two crucial functions in Li-ion batteries: preventing the negative electrode from reducing the electrolyte and permitting Li^+ ions to pass through them. There is extensive literature on SEI films,[34,39] but until recently, almost all of it focused on just three SEI properties: its composition, its formation mechanism, and its impedance. (We note that there is evidence that the impedance that is assigned to the SEI might have contributions from other sources.[136]) In contrast, there is little experimental information about Li transport mechanisms through the SEI—how the SEI actually functions—although at least three different mechanisms have been proposed.[10,76,137] In addition, we are not aware of any measurements of the electrical conductivity of an SEI film,[10] which ideally should be zero but is clearly not, since SEI films inevitably grow. In fact, while tunneling is commonly invoked as a mechanism for electron transport through the SEI,[10,138,139] a thickness of 10 or 20 nm indicates that it must be combined with other mechanisms, as suggested by Qi.[140] To understand battery degradation, we need mechanistic information about how SEI films fail. For example, increased SEI impedance is generally ascribed to its thickness increase,[141,142] as opposed to possible effects of changes in its chemical composition and morphology. There is, thus, little evidence to suggest which chemical components, morphologies, or mechanical properties of an SEI film might be "good" or "bad."

For our initial study of Li^+ transport in the SEI,[75] we used tracer techniques to follow the transport of ions through the solid phase. To simplify the interpretation of our results, we set up experiments that measured Li^+ diffusion, but not migration, and that allowed Li^+ transport into and within the SEI, but not through it. Briefly, we grew SEI films potentiostatically at 0.4 V on a Cu foil substrate in a coin half cell using natural abundance $^7LiClO_4$ as the electrolyte salt. When the current density fell below 1 $\mu A/cm^2$, we removed the foil and rinsed it for a few seconds in DMC to wash away excess $LiClO_4$.[143,144] We then dipped the rinsed SEI for a few minutes in a second electrolyte solution with $^6LiBF_4$ salt, changing both the cation and the anion. During the dip, BF_4^- and $^6Li^+$ ions diffused into the SEI. Finally, we rinsed the sample to remove excess $^6LiBF_4$, transferred it without exposure to air to a TOF-SIMS, and depth profiled through the SEI.

The results for boron are shown in Figure 7a. The SEI thickness is approximately 20 nm, and the boron profile (B^+ or BF_4^-) falls to the baseline within 5 nm. We interpret this to mean that the top 5 nm of the SEI film is porous, at which point it becomes at least locally dense. TOF-SIMS depth profiles show that this outer SEI region is composed largely of polymeric and organic Li salts, chemically distinct from the more inorganic region below it. The presence of a peak for Li_2CO_3 (confirmed by TOF SIMS, TEM, and XPS)[71] at 5 nm suggests that this species or a related one might end the porous region and prevent the boron from penetrating more deeply.

The diffusion of $^6Li^+$ into the SEI shows a very different profile, with the $^6Li/^7Li$ isotope ratio profile plotted in Figure 7b. $^6Li^+$ and BF_4^- must diffuse together to maintain charge balance in the electrolyte, but in the non-porous part of the SEI charge balance can be maintained if any $^6Li^+$ ions that enter are balanced by an equal number of $^7Li^+$ ions that leave, in effect exchanging isotopes. (Because Cu does not react with Li, there is no flux through the SEI.) This logic means that no voltage-driven process affects our measurements since there can be no electrical driving force to exchange isotopes, as Ogletree pointed out (private communication). Thus, the isotope exchange process that we measure must be driven exclusively by diffusion (entropy).

To interpret this rather complex profile Shi et al.[78] suggested a two-zone model in which the dense zone below 5 nm was assumed to be crystalline Li_2CO_3. DFT calculations showed that the dominant defect in this material is interstitial Li and that the dominant diffusion mechanism combines transport via interstitials and Li exchange via a concerted "knock-off" process, in which incoming interstitial $^6Li^+$ ions displace lattice ^7Li ions. The

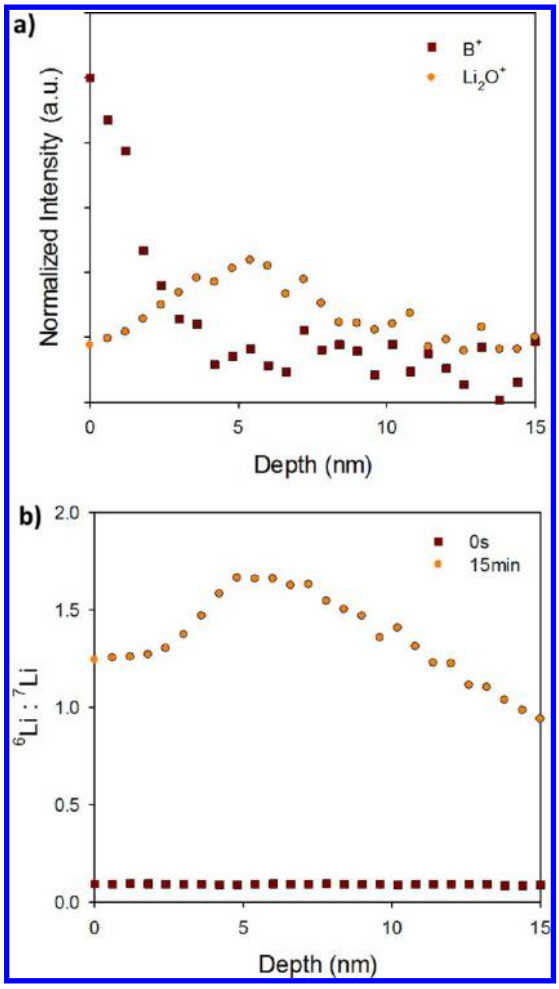

Figure 7. TOF SIMS depth profiles of (a) $^{11}B^+$ and $^7Li_2O^+$ and the (b) ^6Li:^7Li isotope ratio in an SEI film grown in an electrolyte with $^7LiClO_4$ salt; after immersion in $^6LiBF_4$ electrolyte. $^{11}B^+$ and $^7Li_2O^+$ intensities have been normalized to total ion counts, but the isotope ratio values are absolute.

barrier for this knock-off mechanism is only 0.3 eV, significantly below that of other possible transport mechanisms such as hopping. This model explains why the isotope ratio grows without limit within the bulk—because ^6Li replaces ^7Li—and why the isotope ratio falls with depth into the SEI bulk. The intermediate isotope ratio value in the porous region, which is chemically distinct, can be explained if the isotope exchange process there is slower than in the dense part of the SEI. Finally, the high average values for the isotope ratio show that the bulk SEI participates chemically in the transport process. For example, our results are not consistent with a process in which diffusion occurs only via grain boundaries.

For our SEI morphology studies we again used SEI films grown on Cu foil. Four sets of SEI films were formed and studied. The first cell was discharged galvanostatically to 0.7 V and held at this voltage until the current density dropped to <1 $\mu A/cm^2$. The second cell first went through the same procedure as the 0.7 V sample, but after the current dropped below 1 $\mu A/cm^2$ at 0.7 V, we discharged it to 0.5 V and held it there until the current again dropped below 1 $\mu A/cm^2$. Analogous procedures were employed to form SEI films at 0.3 and 0.025 V. This procedure may well produce a different material from an SEI formed by initially setting the voltage at a single value, e.g., 0.025 V, and allowing the current to decay. Our procedure allows us to determine how an SEI that formed, for example, at 0.7 V evolves when the voltage is lowered to 0.5 V, and it may be representative of the very slow formation process used for commercial cells. Depth profiles and SEM images were made for each sample.

From Figure 8a, the SEI thickness, defined by the presence of Li, increased significantly as the voltage was lowered. At the same time, the porosity profile, Figure 8b, extended all the way through the film for voltages of at least 300 mV. (This result, using $LiPF_6$ salt, differs from that described above, where we used $LiClO_4$; in that case, the film became mostly dense by 400 mV.) However, when the voltage is lowered to 25 mV, the porosity profile shrank so that only the first ~5 nm of the film was porous. This suggests that the dense material in the SEI was formed after the porous material, even though the dense material was "below" (closer to the substrate) the porous material. The shrinking of the porosity profile also suggests a conversion of the near-surface porous material to a denser and more reduced material. Simultaneously, the morphology changed dramatically with final voltage, to a dense but cracked (from gas generation, we believe) structure, Figure 8c.

The great majority of SEI studies reported in the literature examined films grown on (realistic) electrode particles, while in our work we studied model SEI films grown on Cu. It is legitimate to ask whether the SEI films we grew are representative of those grown on graphite or other insertion materials. While we cannot give a definitive answer to this question, we offer the following thoughts. (1) Our composition measurements on Cu agree generally with the widely varying compositions observed on graphite. (2) While SEI films grown on the basal planes and prismatic edges of graphite are quite different, the conductivity of graphite in the direction normal to the basal plane is low. This is not the case for either of the prismatic edges of graphite or for Cu. (3) Models of SEI formation[74,83] do not take any account of surface properties yet do a good job explaining the species found. (4) Use of Cu, which does not insert Li, allows us to focus on diffusion into and within the SEI, while excluding effects of insertion. Thus we can be certain that the changes that we see in the SEI at voltages near 300 mV are not related to insertion into anodes, which typically begins in the same voltage range.

■ TOWARD BETTER LI-ION BATTERIES

Homogeneous porous electrode models[6,22] have provided invaluable tools for improving the performance of Li-ion batteries, but the model was not designed to predict durability. We propose that degradation be understood by explicitly considering effects—beneficial or deleterious—of local inhomogeneities on Li^+ transport at larger scales. The value of this hypothesis, if true, is that *it gives a straightforward prescription for making more durable batteries*: control the number and intensity of heterogeneities. While this approach is widely used to make other materials more durable, it is not discussed in the context of Li-ion battery failure.[86]

There is a clear relationship in automotive systems between durability and energy density since durability is achieved partly by oversizing the battery. However, we propose that there is also a more subtle relationship: that the same reduction in variability that can make batteries more durable can also permit an increase in energy density without reducing power density.

Increasing energy density is a top priority for vehicle batteries since a higher energy density translates directly to a greater range. Current research focuses on new electrode chemistries with higher capacity and voltage, but the energy density is the product

dx.doi.org/10.1021/jp311431z | J. Phys. Chem. C 2013, 117, 6481−6492

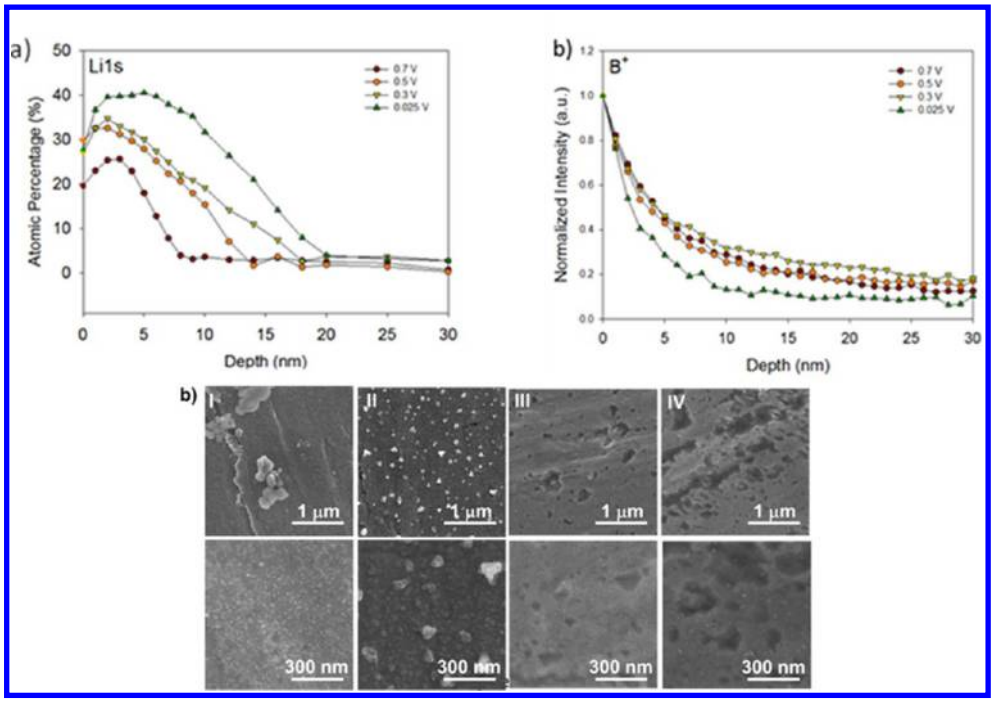

Figure 8. Measurements of SEI films grown at (I) 0.7 V; (II) 0.5 V; (III) 0.3 V; and (IV) 0.025 V. (a) Composition depth profiles (Li 1s). (b) Porosity depth profiles of SEI films. (c) SEM images of SEI .

of three terms: energy density = charge capacity (Ah/kg) × voltage × mass density (kg/L). The third term offers as great an opportunity to improve energy density as the first two terms.[145−148] (Volumetric energy density is more important than gravimetric energy density in commercial systems.) The trade-off between porosity and tortuosity discussed above would seem to preclude increases in density without sacrificing power, but the inverse tortuosity−porosity relationship is a consequence of using a *random* microstructure, such as shown in Figure 9a. There is no reason in principle that *designed* microstructures cannot have simultaneously lower porosity (higher energy density) and lower tortuosity (higher power).[145−148] A simple example of a designed microstructure is shown in Figure 9b, where monodisperse marbles self-assemble into an approximate hexagonal close-packed arrangement (opal structure), filling up to 74% of the volume, compared to ∼60% in a conventional electrode—an improvement of almost 25%. At the same time, the tortuosity of this structure has been measured[132] to be between 2 and 3, significantly below that in many electrodes. Because of the lower τ, thicker electrodes with less inactive components such as current collectors and separators can be made without sacrificing power. Most important from the point of view of our work, we expect that such high energy density cells would experience fewer failures from outlier inhomogeneities such as those shown in Figure 9a or described in Figure 5.

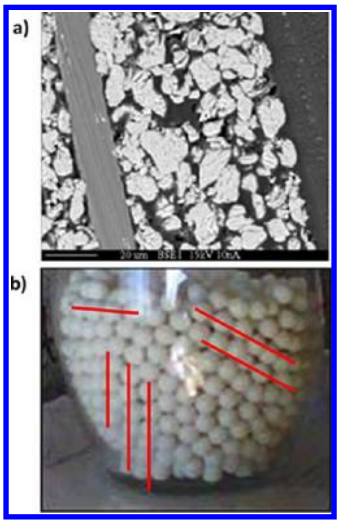

Figure 9. (a) Random microstructure from a $LiCoO_2$ electrode. (b) Self-assembled, nonrandom structure with marbles. Red lines drawn on the figure indicate the presence of (111) planes.

AUTHOR INFORMATION

Corresponding Author

*E-mail: peng.lu@gm.com. Ph: 586-929-3075. Fax: 586-986-1932.

Notes

The authors declare no competing financial interest.

Biographies

Stephen J. Harris received his B.S. in Chemistry at UCLA and his Ph.D at Harvard. This was followed with a Miller Institute Fellowship at

dx.doi.org/10.1021/jp311431z | J. Phys. Chem. C 2013, 117, 6481−6492

Berkeley, after which he spent most of his career at General Motors and Ford Research Laboratories. In 2012 he was a Miller Visiting Professor at Berkeley, and he is now in the Materials Science Division at LBL. His research has encompassed laser diagnostics of combustion, soot formation and aerosol dynamics, chemical vapor deposition of diamond and boron carbide films, contact mechanics modeling and prediction of fatigue lifetimes, microscopic basis for ductile fracture in cast aluminum, and battery degradation.

Peng Lu received his B.S. in Chemistry from Fudan University, Shanghai, in 2004 and his Ph.D in Physical Chemistry from Washington University in St. Louis in 2009. After that, he joined General Motors R&D Center where he is currently a research scientist. He has worked on areas of thin film fabrication and characterization and currently focuses on battery degradation and the battery surface and interfaces.

■ ACKNOWLEDGMENTS

We gratefully acknowledge many valuable conversations with Dr. Mark Verbrugge, Dr. Chen Li, and Dr. Yue Qi at General Motors R&D Center, and Dr. Adam Timmons at Chrysler Corp.

■ REFERENCES

(1) Mizushima, K.; Jones, P.; Wiseman, P.; Goodenough, J. Li_xCoO_2 (0 < x <-1): A New Cathode Material for Batteries of High Energy Density. *Mater. Res. Bull.* **1980**, *15*, 783−789.
(2) Whittingham, M. Chemistry of Intercalation Compounds: Metal Guests in Chalcogenide Hosts. *Prog. Solid State Chem.* **1978**, *12*, 41−99.
(3) Whittingham, M. Lithium Batteries and Cathode Materials. *Chem. Rev.* **2004**, *104*, 4271−4301.
(4) Nagaura, T.; Tozawa, K. Lithium Ion Rechargeable Battery. *Prog. Batteries Solar Cells* **1990**, *9*, 209−217.
(5) Newman, J.; Tobias, C. Theoretical Analysis of Current Distribution in Porous Electrode. *J. Electrochem. Soc.* **1962**, *109*, 1183−1191.
(6) Doyle, M.; Fuller, T.; Newman, J. Modeling of Galvanostatic Charge and Discharge of the Lithium/Polymer/Insertion Cell. *J. Electrochem. Soc.* **1993**, *140*, 1526−1533.
(7) Doyle, M.; Newman, J.; Gozdz, A.; Schmutz, C.; Tarascon, J. M. Comparison of Modeling Predictions with Experimental Data from Plastic Lithium Ion Cells. *J. Electrochem. Soc.* **1996**, *143*, 1890−1903.
(8) Darling, R.; Newman, J. Modeling a Porous Intercalation Electrode with Two Characteristic Particle Sizes. *J. Electrochem. Soc.* **1997**, *144*, 4201−4208.
(9) Srinivasan, V.; Newman, J. Discharge Model for the Lithium Iron-Phosphate Electrode. *J. Electrochem. Soc.* **2004**, *151*, A1517−A1529.
(10) Christensen, J.; Newman, J. A Mathematical Model for the Lithium-Ion Negative Electrode Solid Electrolyte Interphase. *J. Electrochem. Soc.* **2004**, *151*, A1977−A1988.
(11) Srinivasan, V.; Newman, J. Existence of Path-Dependence in the LiFePO4 Electrode. *Electrochem. Solid-State Lett.* **2006**, *9*, A110−A114.
(12) Tang, M.; Newman, J. Electrochemical Characterization of SEI-Type Passivating Films Using Redox Shuttles. *J. Electrochem. Soc.* **2011**, *158*, A530−A536.
(13) Gomadam, P.; Weidner, J.; Dougal, R.; White, R. Mathematical Modeling of Lithium-Ion and Nickel Battery Systems. *J. Power Sources* **2002**, *110*, 267−284.
(14) Ramadass, P.; haran, B.; White, R.; Popov, B. Mathematical Modeling of the Capacity Fade of Li-Ion Cells. *J. Power Sources* **2003**, *123*, 230−240.
(15) Sikha, G.; Popov, B.; White, R. Effect of Porosity on the Capacity Fade of a Lithium-Ion Battery. *J. Electrochem. Soc.* **2004**, *151*, A1104−A1114.
(16) Ploehn, H. J.; Ramadass, P.; White, R. E. Solvent Diffusion Model for Aging of Lithium-Ion Battery Cells. *J. Electrochem. Soc.* **2004**, *151*, A456−A462.
(17) Santhanagoplalan, S.; Guo, Q.; Ramadass, P.; White, R. Review of Models for Predicting the Cycling Performance of Lithium Ion Batteries. *J. Power Sources* **2006**, *156*, 620−628.
(18) Dees, D.; Gunen, E.; Abraham, D.; Jansen, A.; Prakash, J. Alternating Current Impedance Electrochemical Modeling of Lithium-Ion Positive Electrodes. *J. Electrochem. Soc.* **2005**, *152*, A1409−A1417.
(19) Dees, D.; Gunin, E.; Abraham, D.; Jansen, A.; Prakash, J. Electrochemical Modeling of Lithium-Ion Positive Electrodes during Hybrid Pulse Power Characterization Tests. *J. Electrochem. Soc.* **2008**, *155*, A603−A613.
(20) Lopez, C.; Vaughey, J.; Dees, D. Morphological Transitions on Lithium Metal Anodes. *J. Electrochem. Soc.* **2009**, *156*, A726−A729.
(21) Verbrugge, M. W.; Koch, B. J. Electrochemical Analysis of Lithiated Graphite Anodes. *J. Electrochem. Soc.* **2003**, *150*, A374−A384.
(22) Newman, J. Optimization of Porosity and Thickness of a Battery Electrode by Means of a Reaction-Zone Model. *J. Electrochem. Soc.* **1995**, *142*, 97−101.
(23) Guerfi, A.; Kaneko, M.; Petitclerc, M.; Mori, M.; Zaghib, K. $LiFePO_4$ Water-Soluble Binder Electrode for Li-ion Batteries. *J. Power Sources* **2007**, *163*, 1047−1052.
(24) Lux, S. F.; Schappacher, F.; Balducci, A.; Passerini, S.; Winter, M. Low Cost, Environmentally Benign Binders for Lithium-Ion Batteries. *J. Electrochem. Soc.* **2010**, *157*, A320−A325.
(25) Li, C.-C.; Wang, Y.-W. Binder Distributions in Water-Based and Organic-Based LiCoO2 Electrode Sheets and Their Effects on Cell Performance. *J. Electrochem. Soc.* **2011**, *158*, A1361−A1370.
(26) Liu, G.; Xun, S.; Vukmirovic, N.; Song, X.; Olalde-Velasco, P.; Zheng, H.; Battaglia, V. S.; Wang, L.; Yang, W. Polymers with Tailored Electronic Structure for High Capacity Lithium Battery Electrodes. *Adv. Mater.* **2011**, *23*, 4679−4683.
(27) Dominko, R.; Gaberscek, M.; Drofenik, J.; Bele, M.; Pejovnik, S.; Jamnik, J. The Role of Carbon Black Distribution in Cathodes for Li Ion Batteries. *J. Power Sources* **2003**, *119−121*, 770−773.
(28) Verbrugge, M. W.; Koch, B. J. Modeling Li Intercalation of Single Fiber Carbon Microelectrodes. *J. Electrochem. Soc.* **1996**, *143*, 600−608.
(29) Srinivasan, V.; Newman, J. Discharge Model for the Lithium Iron-Phosphate Electrode. *J. Electrochem. Soc.* **2004**, *151*, A1517−A1529.
(30) Zhang, Q.; White, R. E. Moving Boundary Model for the Discharge of a $LiCoO_2$ Electrode. *J. Electrochem. Soc.* **2007**, *154*, A587−A596.
(31) Cheng, Y.-T.; Verbrugge, M. W. Evolution of Stress within a Spherical Insertion Electrode Particle Under Potentiostatic and Galvanostatic Operation. *J. Power Sources* **2009**, *190*, 453−460.
(32) Abraham, D. P.; Knuth, J. L.; Dees, D. W.; Bloom, I.; Christophersen, J. P. Performance Degradation of High-power Lithium-ion Cells—Electrochemistry of Harvested Electrodes. *J. Power Sources* **2007**, *170*, 465−475.
(33) Dees, D.; Gunen, E.; Abraham, D.; Jansen, A.; Prakash, J. Alternating Current Impedance Electrochemical Modeling of Lithium-Ion Positive Electrodes. *J. Electrochem. Soc.* **2005**, *152*, A1409−A1417.
(34) Fedkiw, P.; Newman, J. Friction Factors for Creeping Flow in Sinusoidal Periodically Constricted Tubes. *Chem. Eng. Sci.*, *42*, 2962-2963.

(35) Tang, M.; Albertus, P.; Newman, J. Two-Dimensional Modeling of Lithium Deposition during Cell Charging. *J. Electrochem. Soc.* **2009**, *156*, A390−A399.
(36) Lei, J.; McLarnon, F.; Kostecki, R. In Situ Raman Microscopy of Individual $LiNi_{0.8}Co_{0.15}Al_{0.05}O_2$ Particles in a Li-Ion Battery Composite Cathode. *J. Phys. Chem. B* **2004**, *109*, 952−957.
(37) Panitz, J.; Joho, F.; Novak, P. In Situ Characterization of a Graphite Electrode in a Secondary Lithium-Ion Battery Using Raman Microscopy. *Appl. Spectrosc.* **1999**, *53*, 1188−1199.
(38) Luo, Y.; Cai, W.; Scherson, D. In Situ Raman Spectroscopy of Single Particle Electrodes. *Electrochem. Solid-State Lett.* **2001**, *4*, A101−A104.
(39) Luo, Y.; Cai, W.; Xing, X.; Scherson, D. In Situ, Time-Resolved Raman Spectromicrotopography of an Operating Lithium-Ion Battery. *Electrochem. Solid-State Lett.* **2004**, *7*, E1−E5.
(40) Migge, S.; Sandmann, G.; Rahner, D.; Dietz, H.; Plieth, W. Studying Lithium Intercalation into Graphite Particles via In Situ Raman Spectroscopy and Confocal Microscopy. *J Solid State Electrochem* **2005**, *9*, 132−137.
(41) Novak, P.; Panitz, J.; Joho, F.; Lanz, M.; Imhof, R.; Coluccia, M. Advanced In Situ Methods for the Characterization of Practical Electrodes in Lithium-ion Batteries. *J. Power Sources* **2000**, *90*, 52−58.
(42) Laffont, L.; Delacourt, C.; Gibot, P.; Wu, M.; Kooyman, P.; Masquelier, C.; Tarascon, J. M. Study of the LiFePO4/FePO4 Two-Phase System by High-Resolution Electron Energy Loss Spectroscopy. *Chem. Mater.* **2006**, *18*, 5520−5529.
(43) Yoshizawa, N.; Tanaike, O.; Hatori, H.; Yoshikawa, K.; Kondo, A.; Abe, T. TEM and Electron Tomography Studies of Carbon Nanospheres for Lithium Secondary Batteries. *Carbon* **2006**, *44*, 2558−2564.
(44) Maire, P.; Evans, A.; Kaiser, H.; Scheifele, W.; Novák, P. Colorimetric Determination of Lithium Content in Electrodes of Lithium-Ion Batteries. *J. Electrochem. Soc.* **2008**, *155*, A862−A865.
(45) Hardwick, L.; Buqa, H.; Novak, P. Graphite Surface Disorder Detection Using In Situ Raman Microscopy. *Solid State Ionics* **2006**, *177*, 2801−2806.
(46) Hardwick, L. J.; Holzapfel, M.; Novák, P.; Dupont, L.; Baudrin, E. Electrochemical Lithium Insertion Into Anatase-Type TiO2: An In Situ Raman Microscopy Investigation. *Electrochim. Acta* **2007**, *52*, 5357−5367.
(47) Hardwick, L. J.; Buqa, H.; Holzapfel, M.; Scheifele, W.; Krumeich, F.; Novák, P. Behaviour of Highly Crystalline Graphitic Materials in Lithium-ion Cells with Propylene Carbonate Containing Electrolytes: An In Situ Raman and SEM Study. *Electrochim. Acta* **2007**, *52*, 4884−4891.
(48) http://www1.eere.energy.gov/vehiclesandfuels/about/index.html. Vehicle Technologies Program; content updated 2013, accessed 2013.
(49) Harris, S. J.; Timmons, A.; Pitz, W. J. A Combustion Chemistry Analysis of Carbonate Solvents Used in Li-ion Batteries. *J. Power Sources* **2009**, *193*, 855−858.
(50) Sloop, S. Recycling Advanced Batteries. In *Proceedings of the 2008 IEEE International Symposium on Electronics and the Environment*; IEEE Computer Society: Washington DC, 2008.
(51) Xu, J.; Thomas, H. R.; Francis, R. W.; Lum, K. R.; Wang, J.; Liang, B. A Review of Processes and Technologies for the Recycling of Lithium-ion Secondary Batteries. *J. Power Sources* **2008**, *177*, 512−527.
(52) Armand, M.; Grugeon, S.; Vezin, H.; Laruelle, S.; Ribiere, P.; Tarascon, J. M. Conjugated Dicarboxylate Anodes for Li Batteries. *Nat. Mater.* **2009**, *8*, 120−125.
(53) Huggins, R. *Advanced Batteries: Materials Science Aspects*; Springer Science: New York, 2009.
(54) Smith, A. J.; Burns, J. C.; Trussler, S.; Dahn, J. R. Precision Measurements of the Coulombic Efficiency of Lithium-Ion Batteries and of Electrode Materials for Lithium-Ion Batteries. *J. Electrochem. Soc.* **2010**, *157*, A196−A202.
(55) Smith, A. J.; Burns, J. C.; Zhao, X.; Xiong, D.; Dahn, J. R. A High Precision Coulometry Study of the SEI Growth in Li/Graphite Cells. *J. Electrochem. Soc.* **2011**, *158*, A447−A452.
(56) Andersson, A. M.; Edström, K. Chemical Composition and Morphology of the Elevated Temperature SEI on Graphite. *J. Electrochem. Soc.* **2001**, *148*, A1100−A1109.
(57) Zhang, S.; Ding, M. S.; Xu, K.; Allen, J.; Jow, T. R. Understanding Solid Electrolyte Interface Film Formation on Graphite Electrodes. *Electrochem. Solid-State Lett.* **2001**, *4*, A206−A208.
(58) Jeong, S.-K.; Inaba, M.; Abe, T.; Ogumi, Z. Surface Film Formation on Graphite Negative Electrode in Lithium-Ion Batteries: AFM Study in an Ethylene Carbonate-Based Solution. *J. Electrochem. Soc.* **2001**, *148*, A989−A993.
(59) Kwon, K.; Kong, F.; McLarnon, F.; Evans, J. W. Characterization of the SEI on a Carbon Film Electrode by Combined EQCM and Spectroscopic Ellipsometry. *J. Electrochem. Soc.* **2003**, *150*, A229−A233.
(60) Xu, K.; Zhang, S.; Jow, T. R. Formation of the Graphite/Electrolyte Interface by Lithium Bis(oxalato)borate. *Electrochem. Solid-State Lett.* **2003**, *6*, A117−A120.
(61) Zhuang, G. V.; Ross, P. N. Analysis of the Chemical Composition of the Passive Film on Li-Ion Battery Anodes Using Attentuated Total Reflection Infrared Spectroscopy. *Electrochem. Solid-State Lett.* **2003**, *6*, A136−A139.
(62) Peled, E.; Golodnitsky, D.; Ulus, A.; Yufit, V. Effect of Carbon Substrate on SEI Composition and Morphology. *Electrochim. Acta* **2004**, *50*, 391−395.
(63) Eshkenazi, V.; Peled, E.; Burstein, L.; Golodnitsky, D. XPS Analysis of the SEI Formed on Carbonaceous Materials. *Solid State Ionics* **2004**, *170*, 83−91.
(64) Zhang, H. L.; Li, F.; Liu, C.; Tan, J.; Cheng, H. M. New Insight Into the Solid Electrolyte Interphase with Use of a Focused Ion Beam. *J. Phys. Chem. B* **2005**, *109*, 22205−22211.
(65) Zhang, H.-L.; Li, F.; Liu, C.; Tan, J.; Cheng, H.-M. New Insight into the Solid Electrolyte Interphase with Use of a Focused Ion Beam. *J. Phys. Chem. B* **2005**, *109*, 22205−22211.
(66) Zhao, L.; Watanabe, I.; Doi, T.; Okada, S.; Yamaki, J.-i. TG-MS Analysis of Solid Electrolyte Interphase (SEI) on Graphite Negative-Electrode in Lithium-ion Batteries. *J. Power Sources* **2006**, *161*, 1275−1280.
(67) Bryngelsson, H.; Stjerndahl, M.; Gustafsson, T.; Edström, K. How Dynamic is the SEI? *J. Power Sources* **2007**, *174*, 970−975.
(68) Leroy, S.; Martinez, H.; Dedryvère, R.; Lemordant, D.; Gonbeau, D. Influence of the Lithium Salt Nature over the Surface Film Formation on a Graphite Electrode in Li-ion Batteries: An XPS Study. *Appl. Surf. Sci.* **2007**, *253*, 4895−4905.
(69) Kang, S. H.; Abraham, D. P.; Xiao, A.; Lucht, B. L. Investigating the Solid Electrolyte Interphase using Binder-free Graphite Electrodes. *J. Power Sources* **2008**, *175*, 526−532.
(70) Lu, M.; Cheng, H.; Yang, Y. A Comparison of Solid Electrolyte Interphase (SEI) on the Artificial Graphite Anode of the Aged and Cycled Commercial Lithium Ion Cells. *Electrochim. Acta* **2008**, *53*, 3539−3546.
(71) Tasaki, K.; Goldberg, A.; Lian, J.-J.; Walker, M.; Timmons, A.; Harris, S. J. Solubility of Lithium Salts Formed on the Lithium-Ion Battery Negative Electrode Surface in Organic Solvents. *J. Electrochem. Soc.* **2009**, *156*, A1019−A1027.
(72) Maleki, H.; Howard, J. N. Internal Short Circuit in Li-ion Cells. *J. Power Sources* **2009**, *191*, 568−574.
(73) Verma, P.; Maire, P.; Novák, P. A Review of the Features and Analyses of the Solid Electrolyte Interphase in Li-ion Batteries. *Electrochim. Acta* **2010**, *55*, 6332−6341.
(74) Leung, K.; Budzien, J. L. Ab Initio Molecular Dynamics Simulations of the Initial Stages of Solid Electrolyte Interphase Formation on Lithium Ion Battery Graphitic Anodes. *Phys. Chem. Chem. Phys.* **2010**, *12*, 6583−6586.
(75) Lu, P.; Harris, S. J. Lithium Transport within the Solid Electrolyte Interphase. *Electrochem. Commun.* **2011**, *13*, 1035−1037.
(76) Colclasure, A. M.; Smith, K. A.; Kee, R. J. Modeling Detailed Chemistry and Transport for Solid-Electrolyte-Interface (SEI) Films in Li−ion Batteries. *Electrochim. Acta* **2011**, *58*, 33−43.
(77) Xu, K.; von Cresce, A. Interfacing Electrolytes with Electrodes in Li Ion Batteries. *J. Mater. Chem.* **2011**, *21*, 9849−9864.

(78) Shi, S.; Lu, P.; Liu, Z.; Qi, Y.; Hector, L. G.; Li, H.; Harris, S. J. Direct Calculation of Li-ion Transport in the Solid Electrolyte Interphase. *J. Am. Chem. Soc.* **2012**, *134*, 15476−15487.
(79) Tang, M.; Newman, J. Transient Characterization of Solid-Electrolyte-Interphase Using Ferrocene. *J. Electrochem. Soc.* **2012**, *159*, A281−A289.
(80) Peled, E.; Yamin, H. Solid Electrolyte Interphase (SEI) Electrodes. Part 1. The Kinetics of Lithium in LiAlCl,-SOCl2. *Isr. J. Chem.* **1979**, *18*, 131.
(81) Thevenin, J.; Muller, R. H. Impedance of Li Electrodes in a PC Electrolyte. *J. Electrochem. Soc.* **1987**, *134*, 273−280.
(82) Levi, M. D.; Markevich, E.; Aurbach, D. The Effect of Slow Interfacial Kinetics on the Chronoamperometric Response of Composite Lithiated Graphite Electrodes and on the Calculation of the Chemical Diffusion Coefficient of Li Ions in Graphite. *J. Phys. Chem. B* **2005**, *109*, 7420−7427.
(83) Aurbach, D.; Zinigrad, E.; Cohen, Y.; Teller, H. A Short Review of Failure Mechanisms of Lithium Metal and Lithiated Graphite Anodes in Liquid Electrolyte Solutions. *Solid State Ionics* **2002**, *148*, 405−416.
(84) Patoux, S.; Daniel, L.; Bourbon, C.; Lignier, H.; Pagano, C.; Cras, F.; Jouanneau, S.; Martinet, S. High Voltage Spinel Oxides for Li-ion Batteries: From the Material Research to the Application. *J. Power Sources* **2009**, *189*, 344−352.
(85) Goodenough, J. B.; Kim, Y. Challenges for Rechargeable Li Batteries. *Chem. Mater.* **2010**, *22*, 587−603.
(86) Vetter, J.; Novak, P.; Wagner, M.; Veit, C.; Moller, K.; Besenhard, J.; Winter, M.; Wohlfahrt-Mehrens, M.; Vogler, C.; Hammouche, A. Ageing Mechanisms in Lithium-ion Batteries. *J. Power Sources* **2005**, *147*, 269−281.
(87) Kostecki, R.; McLarnon, F. Local-Probe Studies of Degradation of Composite $LiNi_{0.8}Co_{0.15}Al_{0.05}O_2$ Cathodes in High-Power Lithium-Ion Cells. *Electrochem. Solid-State Lett.* **2004**, *7*, A380−A383.
(88) Hardwick, L. J.; Marcinek, M.; Beer, L.; Kerr, J. B.; Kostecki, R. An Investigation of the Effect of Graphite Degradation on Irreversible Capacity in Lithium-ion Cells. *J. Electrochem. Soc.* **2008**, *155*, A442−A447.
(89) Sethuraman, V. A.; Hardwick, L. J.; Srinivasan, V.; Kostecki, R. Surface Structural Disordering in Graphite upon Lithium Intercalation/Deintercalation. *J. Power Sources* **2010**, *195*, 3655−3660.
(90) Gabrisch, H.; Wilcox, J.; Doeff, M. TEM Study of Fracturing in Spherical and Plate-Like LiFePO4 Particles. *Electrochem. Solid-State Lett.* **2008**, *11*, A25−A29.
(91) Christensen, J.; Newman, J. A Mathematical Model of Stress Generation and Fracture in Lithium Manganese Oxide. *J. Electrochem. Soc.* **2006**, *153*, A1019−A1030.
(92) Itou, Y.; Ukyo, Y. Performance of $LiNiCoO_2$ Materials for Advanced Lithium-ion Batteries. *J. Power Sources* **2005**, *146*, 39−44.
(93) Safari, M.; Delacourt, C. Simulation-Based Analysis of Aging Phenomena in a Commercial Graphite/$LiFePO_4$ Cell. *J. Electrochem. Soc.* **2011**, *158*, A1436−A1447.
(94) Safari, M.; Morcrette, M.; Teyssot, A.; Delacourt, C. Multimodal Physics-Based Aging Model for Life Prediction of Li-Ion Batteries. *J. Electrochem. Soc.* **2009**, *156*, A145−A153.
(95) Aurbach, D.; Zinigrad, E.; Cohen, Y.; Teller, H. A Short Review of Failure Mechanisms of Lithium Metal and Lithiated Graphite Anodes in Liquid Electrolyte Solutions. *Solid State Ionics* **2001**, *148*, 405−416.
(96) Wang, X.; Sone, Y.; Segami, G.; Naito, H.; Yamada, C.; Kibe, K. Understanding Volume Change in Lithium-Ion Cells During Charging and Discharging Using In Situ Measurements. *J. Electrochem. Soc.* **2007**, *154*, A14−A21.
(97) Stux, A.; Swider-Lyons, K. Li-Ion Capacity Enhancement in Composite Blends of $LiCoO_2$ and Li_2RuO_3. *J. Electrochem. Soc.* **2005**, *152*, A2009−A2016.
(98) Guerfi, A.; Kaneko, M.; Petitclerc, M.; Mori, M.; Zaghib, K. $LiFePO_4$ Water-soluble Binder Electrode for Li-ion Batteries. *J. Power Sources* **2007**, *163*, 1047−1052.
(99) Harris, S. J.; Timmons, A.; Baker, D. R.; Monroe, C. Direct In Situ Measurements of Li Transport in Li-ion Battery Negative Electrodes. *Chem. Phys. Lett.* **2010**, *485*, 265−274.
(100) Harris, S. J.; Deshpande, R. D.; Qi, Y.; Dutta, I.; Cheng, Y.-T. Mesopores Inside Electrode Particles Can Change the Li-ion Transport Mechanism and Diffusion-induced Stress. *J. Mater. Res.* **2011**, *25*, 1433−1440.
(101) Kehrwald, D.; Shearing, P. R.; Brandon, N. P.; Sinha, P. K.; Harris, S. J. Local Tortuosity Inhomogeneities in a Lithium Battery Composite Electrode. *J. Electrochem. Soc.* **2011**, *158*, A1393−A1399.
(102) Tvergaard, V. *Adv. Appl. Mech.* **1990**, *27*, 83.
(103) Collins, J. *Failure of Materials in Mechanical design*; John Wiley: New York, 1993.
(104) Holmes, O. W., Sr. *The Deacon's Masterpiece or The Wonderful One-Hoss Shay*. http://www.eldritchpress.org/owh/shay.html, 1858; accessed 2013.
(105) Harris, S. J.; Krauss, G.; Simko, S.; Baird, R.; Gebremaniam, S.; Doll, G. Abrasion and Chemical−Mechanical Polishing Between Steel and a Sputtered Boron Carbide Coating. *Wear* **2001**, *252*, 161−169.
(106) Borodich, F.; Harris, S. J.; Keer, L. Self-similarity in Abrasion of Metals by Nanosharp Asperities of Hard Carbon Containing Films. *Appl. Phys. Lett.* **2002**, *81*, 3476−3478.
(107) Harris, S. J.; O'Neill, A.; Boileau, J.; Donlon, W.; Su, X.; Majumdar, B. Application of the Raman Technique to Measure Stress States in Individual Si Particles in a Cast Al−Si alloy. *Acta Mater.* **2007**, *55*, 1681−1693.
(108) Harris, S. J.; O'Neill, A.; Yang, W.; Gustafson, P.; Boileau, J.; Weber, W.; Majumdar, B.; Ghosh, S. Measurement of the State of Stress in Silicon with Micro-Raman Spectroscopy. *J. Appl. Phys.* **2004**, *96*, 7195−7181.
(109) Dahn, J. R. Phase Diagram of Li_xC_6. *Phys. Rev. B* **1991**, *44*, 9170−9177.
(110) Maire, P.; Kaiser, H.; Scheifele, W.; Novak, P. Colorimetric Determination of Lithium-ion Mobility in Graphite Composite Electrodes. *J. Electroanal. Chem.* **2010**, *644*, 127−131.
(111) Harris, S. J.; Timmons, A.; Baker, D.; Monroe, C. Direct In-Situ Measurements of Li Transport in Li-ion Battery Negative Electrodes. *Chem. Phys. Lett.* **2010**, *485*, 265−274.
(112) Harris, S. J. http://lithiumbatteryresearch.com/LiTransportInGraphiteElectrode.php; content updated 2010, accessed 2013.
(113) Qi, Y.; Harris, S. J. In Situ Observation of Strains during Lithiation of a Graphite Electrode. *J. Electrochem. Soc.* **2010**, *157*, A741.
(114) Kerlau, M.; Marcinek, M.; Kostecki, R. *J. Power Sources* **2007**, *174*, 1046.
(115) Harris, S. J. http://lithiumbatteryresearch.com/StrainMaps.php; content updated 2010, accessed 2013.
(116) Qi, Y.; Guo, H.; Hector, L. G.; Timmons, A. Threefold Increase in the Young's Modulus of Graphite Negative Electrode During Lithium Intercalation. *J. Electrochem. Soc.* **2010**, *157*, A558−A566.
(117) Chen, G.; Song, X.; Richardson, T. J. Electron Microscopy Study of the $LiFePO_4$ to $FePO_4$ Phase Transition. *Electrochem. Solid-State Lett.* **2006**, *9*, A295−A298.
(118) Laffont, L.; Delacourt, C.; Gibot, P.; Wu, M.; Kooyman, P.; Masquelier, C.; Tarascon, J. M. Study of the $LiFePO_4/FePO_4$ Two-Phase System by High-Resolution Electron Energy Loss Spectroscopy. *Chem. Mater.* **2006**, *18*, 5520−5529.
(119) Harris, S. J.; Rahani, E. K.; Shenoy, V. B. Direct In Situ Observation and Numerical Simulations of Non-Shrinking-Core Behavior in an MCMB Graphite Composite Electrode. *J. Electrochem. Soc.* **2012**, *159*, A1501−A1507.
(120) Persson, K.; Sethuraman, V.; Hardwick, L.; Hinuma, Y.; Meng, Y.; van der Ven, A.; Srinivasan, V.; Kostecki, R.; Ceder, G. Li Diffusion in Graphite. *J. Phys. Chem. Lett.* **2010**, *1*, 1176−1180.
(121) Harris, S. J. http://www.youtube.com/watch?v=Y5PEQyoO37M&feature=youtu.be (accessed 2012).
(122) Shearing, P. R.; Howard, L. E.; Jørgensen, P. S.; Brandon, N. P.; Harris, S. J. Characterization of the 3-dimensional Microstructure of a Graphite Negative Electrode from a Li-ion Battery. *Electrochem. Commun.* **2010**, *12*, 374−377.
(123) Vijayaraghavan, B.; Shearing, P. R.; Harris, S. J.; Brandon, N. P.; García, R. E. Electrochemical and Mechanical Reliability of Three

Dimensionally Reconstructed Anode Microstructures. *J. Electrochem. Soc.* **2012**, accepted.
(124) Shearing, P. R.; Brandon, N. P.; Gelb, J.; Bradley, R.; Withers, P. J.; Marquis, A. J.; Cooper, S.; Harris, S. J. Multi Length Scale Microstructural Investigations of a Commercially Available Li-Ion Battery Electrode. *J. Electrochem. Soc.* **2012**, *159*, A1023−A1027.
(125) Thiedmann, R.; Stenzel, O.; Spettl, A.; Shearing, P. R.; Harris, S. J.; Brandon, N. P.; Schmidt, V. Stochastic Simulation Model for the 3D Morphology of Composite Materials in Li−ion Batteries. *Comput. Mater. Sci.* **2011**, *50*, 3365−3376.
(126) Wilson, J. R.; Cronin, J. S.; Barnett, S. A.; Harris, S. J. Measurement of Three-Dimensional Microstructure in a $LiCoO_2$ Positive Electrode. *J. Power Sources* **2011**, *196*, 3443−3447.
(127) Lanzi, O.; Landau, U. Effect of Pore Structure on Current and Potential Distributions ina Porous Electrode. *J. Electrochem. Soc.* **1990**, *137*, 585−593.
(128) Thorat, I. V.; Stephenson, D. E.; Zacharias, N. A.; Zaghib, K.; Harb, J. N.; Wheeler, D. R. Quantifying Tortuosity in Porous Li-ion Battery Materials. *J. Power Sources* **2009**, *188*, 592−600.
(129) Verbrugge, M.; Koch, B. Electrochemical Analysis of Lithiated Graphite Anodes. *J. Electrochem. Soc.* **2003**, *150*, A374−A384.
(130) Shen, L.; Chen, Z. Critical Review of the Impact of Tortuosity on Diffusion. *Chem. Eng. Sci.* **2007**, *62*, 3748−3755.
(131) Zalc, J. M.; Reyes, S. C.; Iglesia, E. The Effects of Diffusion Mechanism and Void Structure on Transport Rates and Tortuosity Factors in Complex Porous Structures. *Chem. Eng. Sci.* **2004**, *59*, 2947−2960.
(132) Newton, M.; Morey, K.; Zhang, Y.; Snot, R.; Diwekar, M.; Shi, J.; White, H. Anisotropic Diffusion in FCC Opals. *Nano Lett.* **2004**, *4*, 875−880.
(133) Tomadakis, M.; Sotirchos, S. Transport Porperties of Random Arrays of Freely Overlapping Cylinders with Various Orientation Distributions. *J. Chem. Phys.* **1983**, *98*, 616−626.
(134) Garcia, E.; Chiang, Y. Spatially Resolved Modeling of Microstructurally Complex Battery Architectures. *J. Electrochem. Soc.* **2007**, *154*, A856−A864.
(135) Zhang, H.; Li, F.; Liu, C.; Tan, J.; Cheng, H. New Insight into the Solid Electrolyte Interphase with Use of a Focused Ion Beam. *J. Phys. Chem. B* **2005**, *109*, 22205−22211.
(136) Kerlau, M.; Marcinek, M.; Srinivasan, V.; Kostecki, R. M. Studies of Local Degradation Phenomena in Composite Cathodes for Lithium-ion Batteries. *Electrochim. Acta* **2007**, *52*, 5422−5429.
(137) Peled, E.; Golodnitsky, D.; Ardel, G. Advanced Model for Solid Electrolyte Interphase Electrodes in Liquid and Polymer Electrolytes. *J. Electrochem. Soc.* **1997**, *144*, L208−L210.
(138) Weinstein, L.; Yourey, W.; Gural, J.; Amatucci, G. G. Electrochemical Impedance Spectroscopy of Electrochemically Self-Assembled Lithium−Iodine Batteries. *J. Electrochem. Soc.* **2008**, *155*, A590−A598.
(139) Xu, K.; von Cresce, A.; Lee, U. Differentiating Contributions to ″Ion Transfer″ Barrier from Interphasial Resistance and Li^+ Dsolvation at Electrolyte/Graphite Interface. *Langmuir* **2010**, *26*, 11538−11543.
(140) Qi, Y. Private Communication, 2012.
(141) Peled, E. The Electrochemical Behavior of Alkali and Alkaline Earth Metals in Nonaqueous Battery Systems–The Solid Electrolyte Interphase Model. *J. Electrochem. Soc.* **1979**, *126*, 2047−2051.
(142) Broussely, M.; Herreyre, S.; Biensan, P.; Kasztenjna, P.; Nechev, K.; Staniewicz, R. Aging Mechanism in Li Ion Cells and Calendar Life Predictions. *J. Power Sources* **2001**, *97*, 13−21.
(143) Tasaki, K.; Goldberg, A.; Lian, J.; Walker, M.; Timmons, A.; Harris, S. J. Solubility of Lithium Salts Formed on the Lithium-Ion Battery Negative Electrode Surface in Organic Solvents. *J. Electrochem. Soc.* **2009**, *156*, A1019−A1027.
(144) Tasaki, K.; Harris, S. J. Computational Study on the Solubility of Lithium Salts Formed on Lithium Ion Battery Negative Electrode in Organic Solvents. *J. Phys. Chem. C* **2010**, *114*, 8076−8083.
(145) Chiang, Y. M. New Electrode Designs for Ultrahigh Energy Density. In *DOE Annual Merit Review*; Massachusetts Institute of Technology: Cambridge, MA, 2011.
(146) Lai, W.; Erdonmez, C.; Marinis, T.; Bjune, C.; Dudney, N. J.; Xu, F.; Wartena, R.; Chiang, Y. M. Ultrahigh-Energy-Density Microbatteries Enabled by New Electrode Architecture and Micropackaging Design. *Adv. Mater.* **2010**, *22*, E139−E144.
(147) Tarascon, J. M. Key Challenges in Future Li-battery Research. *Philos. Trans. A, Math. Phys. Eng. Sci.* **2010**, *368*, 3227−3241.
(148) Zhang, H.; Yu, X.; Braun, P. V. Three-Dimensional Bicontinuous Ultrafast Charge and Discharge Bulk Battery Electrodes. *Nat. Nanotechnol.* **2011**, *6*, 277−281.